Am J Nucl Med Mol Imaging 2018;8(6):397-406
www.ajnmmi.us /ISSN:2160-8407/ajnmmi0087675

Original Article

Evaluation of planar bioluminescence imaging and microPET/CT for therapy monitoring in a mouse model of pigmented metastatic melanoma

Ewa Pasquereau-Kotula[1], Benoit Hosten[2,3], Fortune Hontonnou[2,4], Nicolas Vignal[2,3], Florent Antoni[2], Jean-Luc Poyet[1], Nathalie Rizzo-Padoin[2,3], Laure Sarda-Mantel[2,4,5]

[1]Inserm UMR-S1160, [2]Unité Claude Kellershohn, Institut Universitaire d'Hématologie, Hôpital St-Louis, Paris, France; [3]Inserm UMR-S1144, Faculté de Pharmacie, Université Paris Descartes, Paris, France; [4]Université Paris Diderot, Paris, France; [5]Inserm UMR-S942, Hôpital Lariboisière, Paris, France

Received August 21, 2018; Accepted November 21, 2018; Epub December 20, 2018; Published December 30, 2018

Abstract: Bioluminescence imaging (BLI) is widely used for *in-vivo* monitoring of anti-cancer therapy in mice. [^{18}F]MEL050 is a Positron Emission Tomography (PET) radiotracer which specifically targets melanin. We evaluated planar BLI and [^{18}F]MEL050-PET/CT for therapy (pro-apoptotic peptide LZDP) monitoring in a mouse model of metastatic pigmented melanoma. Twelve B6-albino mice were intravenously injected with B16-F10-luc2 cells on day 0 (D0). The mice received daily from D2 to D17 either an inactive peptide (G1, n=6), or LZDP (G2, n=6). They underwent both BLI and [^{18}F]MEL050-PET/CT imaging on D2, D8 and D17. The number of visible tumors was determined on BLI and PET/CT. [^{18}F]MEL050 uptake in tumor sites was quantified on PET/CT. After sacrifice (D17), the number of black tumors was counted *ex-vivo.* On D2, BLI and PET/CT images were visually negative. On D8, BLI detected 8 tumor sites in 4/6 mice of G1 vs 5 in 3/6 mice of G2 (NS); PET/CT was visually negative. On D17, BLI detected 17 tumor sites in 5/6 mice of G1 vs 10 in 4/6 mice of G2 (NS). PET/CT detected 18 tumor sites in 4/4 mice of G1 vs 14 in 3/4 mice of G2 (NS). Mean %ID/g of [^{18}F]MEL050 in tumor sites was lower in G2 than in G1 on D17 ($P<0.001$), whereas bioluminescence intensity was not different between the 2 groups. *Ex-vivo* examination confirmed lower number of tumors in G2 ($P<0.03$). In the small number of animals tested in this study, [^{18}F]MEL050-PET/CT and *ex-vivo* examination could affirm anti-tumoral effect of LZDP, but not BLI.

Keywords: Bioluminescence imaging, microPET/CT, therapy assessment, melanoma, murine metastatic model

Introduction

Melanoma is a highly malignant tumor of pigment-producing cells (melanocytes). The incidence rate of melanoma has more than tripled in the white population during the last 30 years and it continues to rise worldwide. In 2016, it is estimated that there will be 76,380 new cases of melanoma of the skin and an estimated 10,130 people will die of this disease in the United States [1]. The ongoing trend of rising melanoma incidence rates in most white populations is projected to continue over the next two to three decades. In France, cutaneous melanoma is the 11th most common cancer in both sexes, with an estimation of 14,325 new cases in 2015 [2]. Although early detection, appropriate surgery, and adjuvant therapy have improved outcomes, the prognosis of metastatic melanoma remains very poor. Advanced melanoma is still associated with an extremely poor median survival, ranging from 2 to 8 months, with only 5% surviving more than 5 years and remains one of the most treatment-refractory malignancies. Many agents have been investigated for antitumor activity in melanoma but the current treatment options for patients with metastatic disease are limited and non-curative in the majority of cases [3]. Conventional treatments for melanoma, including chemotherapy, radiation therapy or immunotherapy are associated with low progression-free survival rates and impaired by significant adverse effects. The 3-year survival rate is less than 15% [4]. Targeted therapies such as Braf inhibitors are under evaluation with encourag-

ing results [5]. However the search for new therapeutics is a major public health issue.

JL Poyet's team chose to target anti-apoptotic AAC-11 (or Api5, or fibroblast growth factor-2-interacting factor (FIF)) protein, which is overexpressed in malignant melanoma as well as in several cancer types, and is associated with poor prognosis and with metastatic phenotype. AAC-11 is implied in the resistance to anti-cancer therapy including radiotherapy [6]. Especially, AAC-11 inhibits apoptosis related to transcription factor E2F1. It is a nuclear protein comprising 510 aa highly stable between species. AAC-11 knock-out is lethal in several cell lines during nutritional stress [7], suggesting a role of AAC-11 in cell survival. Cells that overexpress AAC-11 resist to stimuli which induce apoptosis, such as chemotherapy, radiotherapy, growth factor deprivation, and death receptors activation [8]. Such protein is thus an interesting target for the development of new anti-cancer strategies. Especially JL Poyet et al. previously showed that the administration of an AAC-11-inhibiting peptide (LZDP) induced selectively cancer cell death in a murine model of metastatic pigmented melanoma [9].

In the present study, we followed the effect of LZDP *in vivo* in this latter murine model, by using two *in-vivo* imaging modalities, planar bioluminescence imaging (BLI) and Positron Emission Tomography coupled to X-rays computed tomography (PET/CT). BLI is widely used to evaluate non invasively antitumor effects of treatments in animal models [9, 10]. MicroPET/CT has also been described as an accurate tool to monitor biological effects and effectiveness of antitumor treatments *in-vivo* in animal models [11, 12]. It is not known if microPET/CT has additional value as compared to planar BLI in this setting. [^{18}F]FDG Positron Emission Tomography (PET) imaging is routinely used for initial staging of III/IV malignant melanoma (detection of distant metastases), and seems to be useful for therapeutic follow-up [13]. Besides [^{18}F]FDG, radiolabelled benzamide derivatives appear as interesting compounds for sensitive detection of pigmented malignant melanomas. They exhibit high and specific binding with melanin in melanoma cells and melanocytes [14]. Promising results were obtained with these benzamide derivatives for both diagnosis and therapeutic applications [15]. Clinical trials have shown the usefulness of ^{123}I-BZA and ^{123}I-BZA2 for the detection of melanoma and its metastases with high specificity and sensitivity [16]. MEL050 is one of the synthetic benzamide derived molecules that specifically binds to melanin with high affinity. Melanin is highly expressed in pigmented melanoma so we and others used MEL050 as a PET tracer for this tumor type after radiolabelling with F-18 in experimental models [17]. Indeed we previously demonstrated high sensitivity of [^{18}F]MEL050-PET/CT for tumor detection in mice with B16F10luc2 Luciferase expressing pigmented xenografts and metastases [18].

In the present study, we evaluated BLI and [^{18}F]MEL050-PET/CT for *in-vivo* non invasive assessment of LZDP efficacy in the metastatic model of pigmented melanoma.

Methods

Study design

Lung and bone metastases of pigmented melanoma were induced by iv injection of 500000 B16F10luc2 cells in 2 groups of B6-albino mice on day 0. The treatments were started 48 h after the induction of the model (day 2). Mice of group 1 (G1: control group) received 15 doses of an inactive peptide (5 mg/kg ip per day, from day 2 to day 17); mice of group 2 (G2: treated group) received 15 doses of active AAC-11 inhibiting peptide LZDP (5 mg/kg ip per day, from day 2 to day 17). All animals underwent two *in-vivo* imaging procedures at three time points: on day 2 (before treatment), then on day 8, then on day 17. After imaging on day 17, the mice were dissected and the number of tumor lesions (black nodules) was counted.

All animal experiments were performed in accordance with European Guidelines for Care of laboratory Animals (2010/63/EU) and were approved by the Animal Ethics Committee of Paris Nord.

Peptides

Peptides were synthesized by Proteogenix (Strasbourg, France) and were > 95% pure as determined by HPLC and mass spectrographic analysis. Active peptide is called LZDP. Inactive peptide is a variant of the active one but with no biological activity.

Cell cultures

The B16-F10-luc2 cells (murine melanoma cells, Caliper life sciences, USA) were kindly provided by Dr. Marie Dutreix (Institut Curie, France). Cell cultures were maintained as monolayers in RPMI 1640 (Gibco, Cergy Pontoise, France) medium containing 10% heat-inactivated Fetal Bovine Serum (Gibco) and antibiotics (100 mg/mL streptomycin and 100 mg/mL penicillin; Gibco). The cells were grown at 37°C in a humidified incubator containing 5% CO_2.

Animal model

Metastases of pigmented melanoma were induced by injection of 0.5×10^6 B16-F10-luc2 cells in 100 µL of PBS into the lateral tail vein of 7 weeks old B6-albino mice (n=6 per group), as previously described [18].

Bioluminescence imaging

Planar BLI was performed as previously described using the IVIS Spectrum imaging system (Perkin Elmer) (n=12) [5]. Intra-peritoneal injection of luciferin (15 mg/mL, 0.2 mL) was performed under anesthesia with isoflurane/oxygen, 2.5%. Fifteen minutes later the mice were placed in the IVIS chamber for imaging. Anesthesia was continued during the procedure with 2% isoflurane/oxygen introduced via a nose cone. Planar anterior images were acquired with 300 s exposure time, which did not induce signal saturation (the acquisition system comprises a warning message when signal saturation is reached).

MicroPET/CT

[^{18}F]MEL050 radiosynthesis: Radiosynthesis of [^{18}F]MEL050 was performed as previously described [18].

Briefly it was performed on an AllInOne™ synthesis module using an in-house reaction sequence, using one-step bromine-for-fluorine nucleophilic heteroaromatic substitution, inspired by previous publications [19, 20].

The aqueous [^{18}F]fluoride target solution was loaded on a QMA (Pre-conditioned Sep-Pak® Light QMA cartridge, ABX). The concentrated [^{18}F]fluoride was eluted into the reactor using a K_2CO_3 (3 mg) and Kryptofix (K222, 15 mg) mixed solution (1 mL, CH_3CN/H_2O, 80:20, v/v). The solvents were evaporated under reduced pressure at 110°C for 7 min. To the dry residue containing the K222/potassium [^{18}F]fluoride complex was added the bromo precursor (2 mg) in DMF (1 mL) and the mixture was heated and maintained at 150°C for 6 min. After cooling, the HPLC mobile phase (2.5 mL) was added to the reaction mixture. The resulting solution was injected onto semi-preparative HPLC system. The fraction containing [^{18}F]MEL050, associated to a well-defined radioactive peak was collected at 10-12 min. The collected fraction was diluted with 20 mL of water, and the resulting solution passed through a C18 cartridge (Sep-Pak® Plus C18 environmental, Waters). The cartridge with radioactive product retained was washed with water (10 mL) before being eluted with 1 mL of ethanol and then 10 mL of saline. The radiotracer solution was finally passed through a 0.22 µm Millipore filter into a sterile vial for *in-vivo* experiments.

The radiochemical and chemical purity, stability and specific activity measurements were performed by analytical HPLC. The specific activity of the radiotracer was assessed by measurement of the radioactivity injected and the MEL050 concentration in the sample, derived from the UV detection. The identity of the labeled compound [^{18}F]MEL050 was confirmed by co-injection with a non-radioactive standard of MEL050. The MEL050 concentration in the radioactive sample was obtained using the UV-peak area ratio between the radioactive product and the standard solution.

[^{18}F]MEL050-PET/CT imaging

PET/CT imaging was performed as previously described using Inveon PET/CT scanner (Siemens Medical Solutions) designed for small laboratory animals [18]. Mice were anesthetized (isoflurane/oxygen, 2.5% for induction at 0.8-1.5 L/min and 1.5% at 0.4-0.8 L/min thereafter) during injection of [^{18}F]MEL050 (7.3±0.6 MBq) in a volume of 0.15 mL via the tail vein, and during PET/CT acquisitions.

Mice were kept in standby for 1 hour after radiotracer injection, then were re-anesthetized and placed in the PET camera in prone position under isoflurane anesthesia and respiratory monitoring for a 20 min-duration static PET acquisition. Then a 10 min-duration CT acquisition was performed for attenuation correction

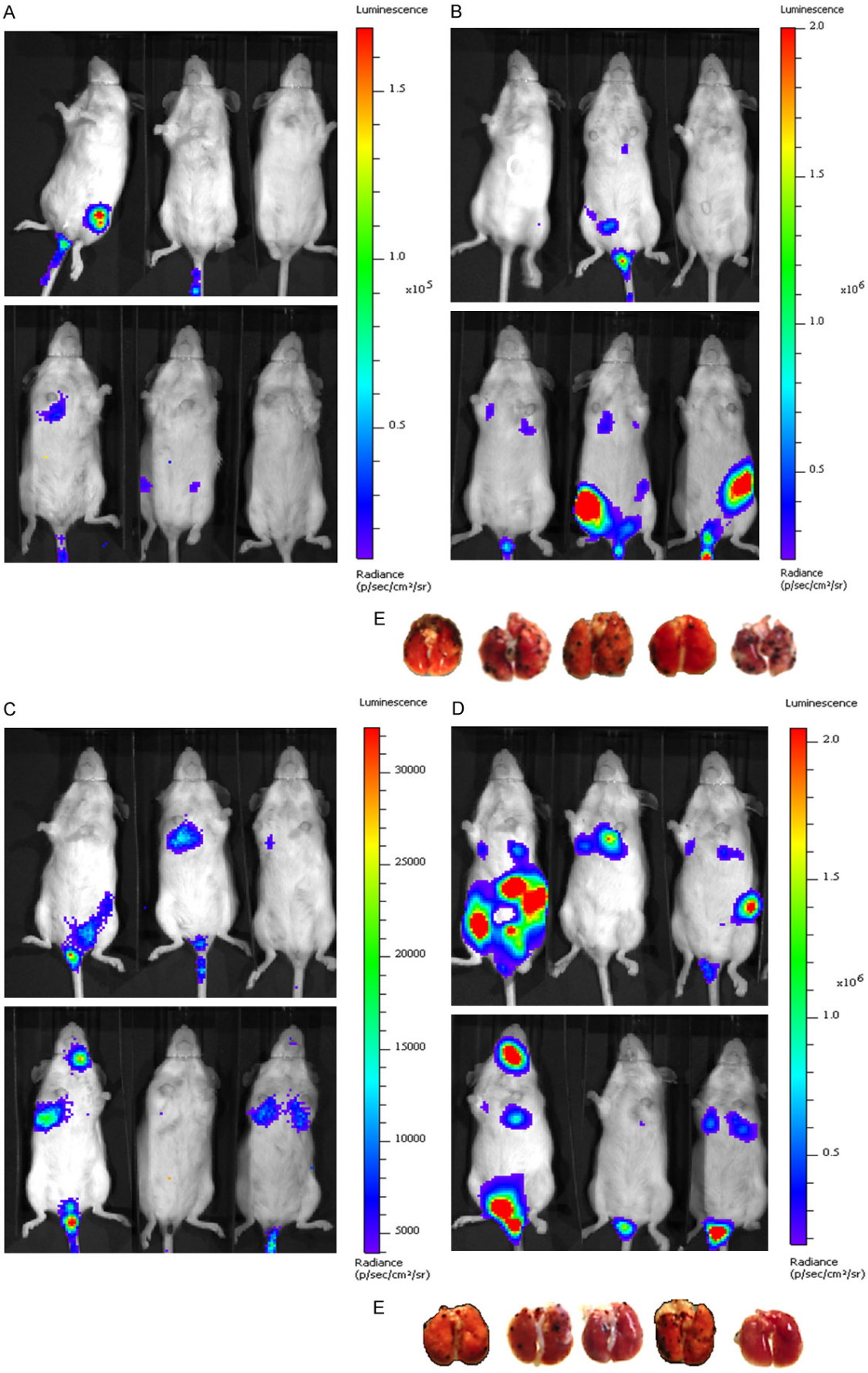
A
Luminescence
1.5
1.0
x10^5
0.5
Radiance (p/sec/cm²/sr)
B
Luminescence
2.0
1.5
x10^6
1.0
0.5
Radiance (p/sec/cm²/sr)
E
C
Luminescence
30000
25000
20000
15000
10000
5000
Radiance (p/sec/cm²/sr)
D
Luminescence
2.0
1.5
x10^6
1.0
0.5
Radiance (p/sec/cm²/sr)
E

Figure 1. Bioluminescence IVIS images and lungs *ex-vivo.* A: BLI of control group on day 8; B: BLI images of control group on day 17. C: BLI of treated group on day 8; D: BLI images of treated group on day 17. E: Extracted lungs of control group (top) and of treated group (bottom); tumor lesions appear as black nodules.

of PET images and anatomic localization of PET hot spots, according to the methodology described by Denoyer et al. [17].

The spatial resolution of Inveon PET device was 1.4 mm full-width at half-maximum at the center of the field of view. Images were reconstructed using a 2-D ordered subset expectation maximization (Fourier rebinning/2-D OSEM) method including corrections for scanner dead time, scatter radiations and randoms.

Data analysis

BLI and PET/CT images were visually assessed (number of visible hot spots). Then quantitative analysis of PET/CT images was performed by drawing volumes of interest involving the whole lungs and extra-pulmonary hot spots for quantification of radiotracer uptakes in tumor sites.

All values of radioactivity concentrations were normalized by the injected dose and expressed as percentage of the injected dose per g of tissue (%ID/g). These %ID/g in volumes of interest (right and left lungs, extra-pulmonary hot spots) were obtained on 20 min duration static acquisition images performed 1 hour after injection. They were analyzed using Inveon Research Workplace 4.2 software. The software calculates %ID/g in each voxel of the volumes of interest drawn on the images. The mean and max %ID/g values obtained in the volumes of interest (in each 20 minutes duration static acquisition image) were considered for quantitative analysis as performed with standardized uptake value (SUV) in patients.

Statistical analysis

Data are presented as mean ± SD: Statistical analysis was performed using Graphpad prism 5 version 5.0 software. Wilcoxon signed-rank test was used to compare the number of tumors, bioluminescence intensity (photon/s/cm^2/sr) as well as mean and max %ID/g of [^{18}F]MEL050 in tumor sites obtained in untreated and treated groups on day 2, day 8 and day 17. A significance value of $P<0.05$ was used.

Results

All the mice were kept alive during the whole procedure and underwent planar BLI. For technical reasons (failure of intraveinous radiotracer injection), 4 of 6 mice per group underwent [^{18}F]MEL050-PET/CT imaging.

[^{18}F]MEL050 was produced in greater than 99% radiochemical purity, the activity concentration varied with the range of 0.91-1.95 GBq/ml. The specific activity was within the range of 177-325 GBq/μmol and the radiochemical purity was maintained at > 98% over 6 h in saline.

On day 2, before treatments, all BLI and PET/CT images were visually negative in the two groups.

After 7 doses (on day 8), BLI detected 8 tumor sites in 4/6 mice of G1 vs 4 tumor sites in 3/6 mice of G2 (NS): 5 lung lesions, 1 mandibular and 2 in the flanks for G1, 1 lung lesion and 3 in the flanks for G2 (**Figure 1**). CT images revealed 1 lung nodule (0.5 mm) in 2/4 mice of G1 and in 2/4 mice of G2. PET/CT images were negative on visual analysis (no visible hot spot). Mean %ID/g of [^{18}F]MEL050 in the lungs was 0.94±0.15 in G1 vs 0.80±0.13 in G2 (NS). Max %ID/g of [^{18}F]MEL050 in the lungs was 1.85±0.26 in G1 vs 1.69±0.42 in G2 (NS) (**Figure 2**).

After 15 doses (on day 17), BLI detected 17 tumor sites in 5/6 mice of G1 vs 10 in 4/6 mice of G2 on day 17 (NS): 11 lung lesions, 1 mandibular, 5 in the flanks for G1, 5 lung lesions and 5 in the flanks for G2 (**Figure 1**). PET/CT detected 17 tumor sites in 4/4 mice of G1 vs 14 in ¾ mice of G2 (NS). It missed 1 lung lesion seen on BLI and discovered 5 tumor sites not seen on BLI (4 lung nodules and 1 bone metastasis). **Figure 2** shows a deep infra-millimetric lung tumor seen on PET/CT imaging and not detectable with BLI. PET/CT allowed precise localization of extra-pulmonary lesions which corresponded to lymph nodes, mandibular and femoral bone tumor lesions.

Tumor amounts measured on BLI imaging were not often concordant with those evidenced on PET/CT. For example in **Figure 3** a small femo-

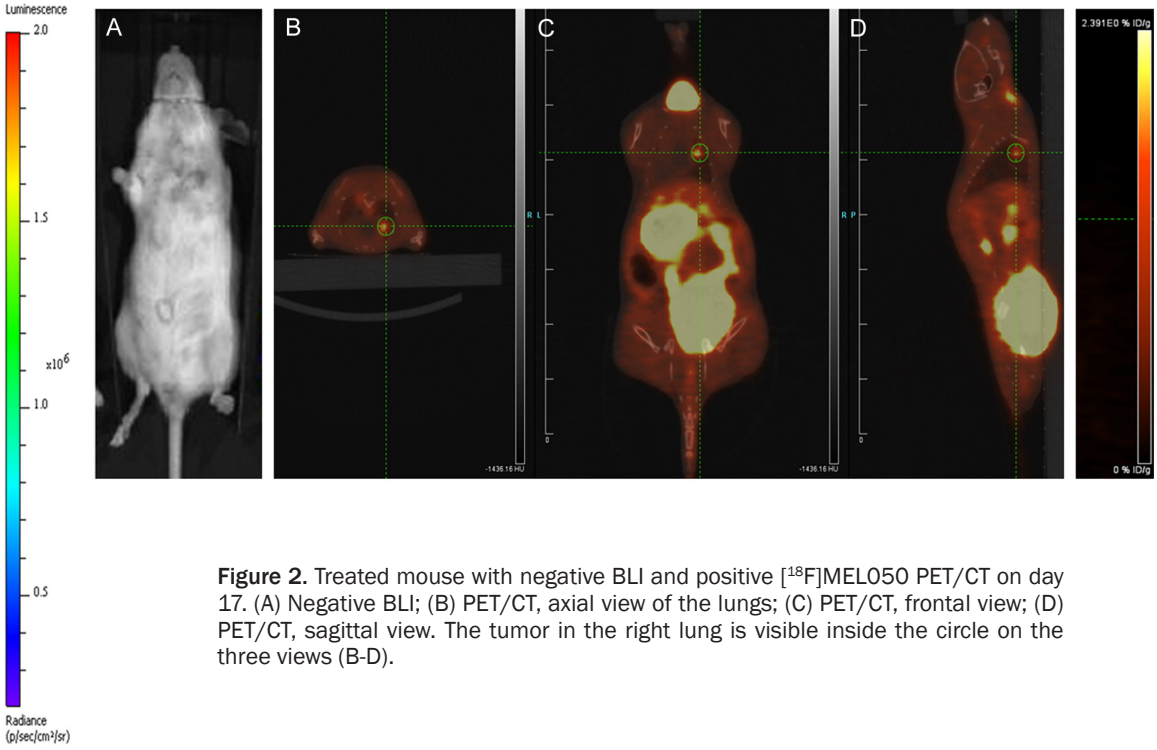

Figure 2. Treated mouse with negative BLI and positive [^{18}F]MEL050 PET/CT on day 17. (A) Negative BLI; (B) PET/CT, axial view of the lungs; (C) PET/CT, frontal view; (D) PET/CT, sagittal view. The tumor in the right lung is visible inside the circle on the three views (B-D).

ral bone tumor evidenced on PET/CT appeared very strong and large on BLI. BLI signals (Photons/sec/cm^2/sr) in the lungs were significantly lower in G2 than in G1 on day 17 (29153±32096 vs 139328±94435, P<0.02), but the difference was not significant when all lung and extrapulmonary tumor lesions were considered (211907±269219 vs 256217±269219, NS) (**Figure 4** right). Conversely mean %ID/g of [^{18}F]MEL050 was significantly lower in G2 than in G1 in the lungs (0.97±0.13 vs 1.37±0.23 P<0.001), and also when all lung and extra-pulmonary lesions were considered (1.19±0.38 vs 1.81±1.38 P<0.05) (**Figure 4** left). Max %ID/g was not significantly lower in G2 than in G1: 3.03±2.17 vs 4.94±4.38 (NS) in the lungs, and 3.35±2.61 vs 4.82±4.77 (NS) in lung and extra-pulmonary lesions.

On day 17, *ex-vivo* examination confirmed lower number of black tumors in the treated group than in the control group: 14±11 vs 39±26, P<0.05. Most lesions were found in the lungs (**Figure 1**).

Discussion

In this study performed in a small number animals, BLI, micro [^{18}F]MEL050-PET/CT and *ex-vivo* examination retrieved lower tumor involvement in the treated group than in the control group. But the difference reached statistical significance only on PET/CT imaging and on *ex-vivo* examination. Quantification of luminescence was not relevant in this model. PET/CT allowed precise localization of extra-pulmonary lesions.

In preclinical studies, the evaluation of new antitumor therapies is classically based on *ex-vivo* counting and histobiological characterization of tumors at the end of therapy courses. Non-invasive *in-vivo* imaging methods can also be used during therapeutic courses in this setting.

In mice models grafted with genetically modified luciferase expressing lineages of tumors, the most widely *in-vivo* imaging method used is BLI, which is based on the detection of light emission induced in tumor cells by the action of transgenic luciferase on ip injected substrate luciferin [9, 10, 21].

PET/CT is of interest in clinical practice for longitudinal monitoring of antitumor therapies especially in lymphomas, as a marker of treatment efficacy at the end of the therapeutic

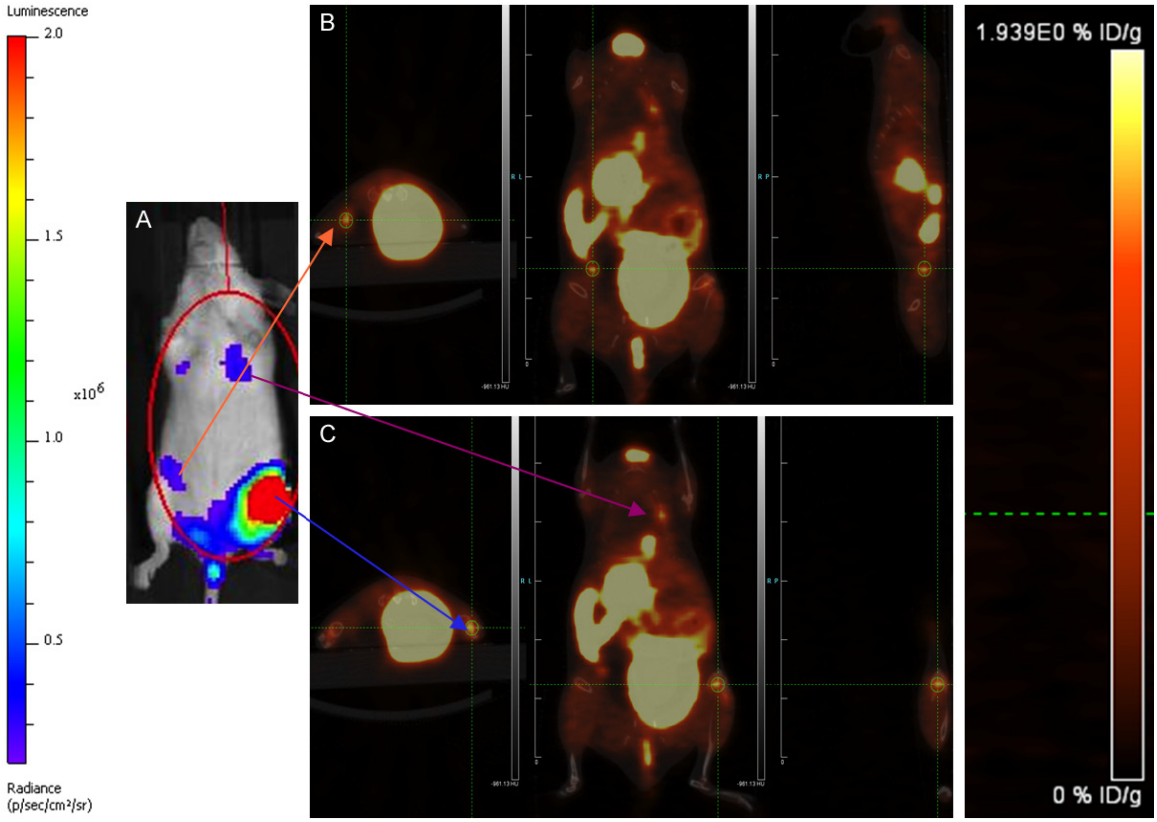

Figure 3. Example of BLI and [^{18}F]MEL050 PET/CT imaging in a treated mouse on day 17. A: BLI showing lesions in both lungs and in the right and the left flanks; B: PET/CT: axial, frontal and sagittal views of the tumoral lymph node (inside the circle) corresponding to the lesion of the right flank on BLI (arrow); C: PET/CT: axial, frontal and sagittal views of right femur bone metastasis (inside the circle) corresponding to the lesion of the left flank on BLI (arrow): BLI signal overestimates the size of this lesion; the lesion in the left lung is visible on PET/CT (arrow) whereas that in the right lung (visible on BLI) is not detected with PET/CT.

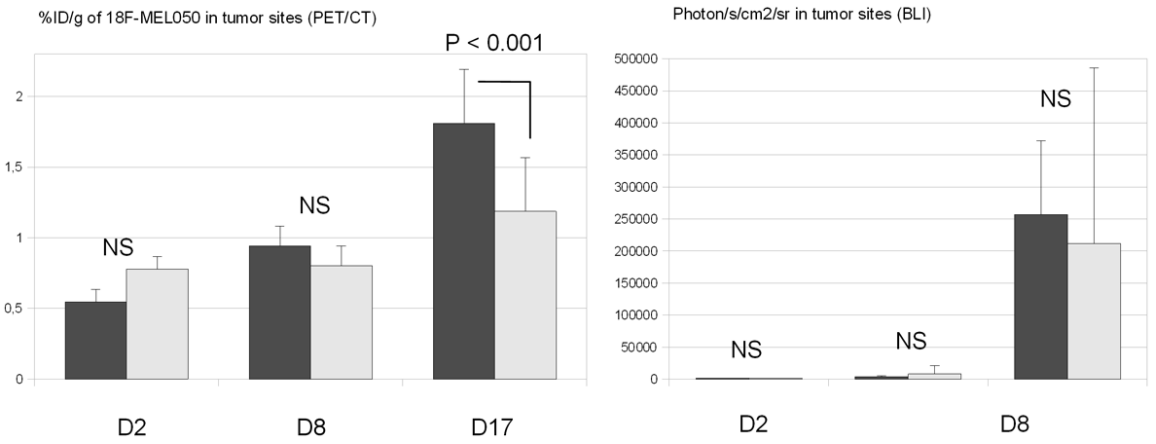

Figure 4. PET and BLI quantification in all tumor sites on days 2, 8 and 17 in control (G1, black rectangles, n=4) and treated (G2, white rectangles, n=4) groups. Left: Mean %ID/g, significantly lower value after 15 doses in G2 than in G1. Right: Photons/sec/cm^2/sr, no significant difference between groups at any time.

course [22, 23], and as an early predictor of treatment efficacy after 1 or 2 cycles of chemotherapy [24]. PET/CT is also of interest for treatment response assessment and radiation therapy personalization in lung cancers [25]. More recently microPET/CT has also been used for

longitudinal follow-up of various tumor types in murine models [11, 12, 26-31], for *in-vivo* evaluation of tumor expansion/spreading and/or biological characterization.

We previously demonstrated that [^{18}F]MEL050-PET/CT is highly sensitive for tumor detection in murine models of pigmented melanoma xenografts and lung metastases [5]. In the present study we evaluated BLI and [^{18}F]MEL050-PET/CT for LZDP anti-tumor effect assessment in the latter metastatic model.

Photon emissions during luminescence and positron emission have different energy characteristics: visible light low energy photons for bioluminescence imaging, very high energy photons for PET imaging. Therefore luminescent photons have a very small course before they are entirely absorbed in the animals, whereas PET emitters' high energy photons almost don't interact with animal body before detection. This can explain the case illustrated in **Figure 2** of a deep and very small lung tumor visible on PET images but not detected with BLI. Conversely in a small bone tumor of the knee precisely assessed on PET/CT (**Figure 3**), BLI signal was very intense and large, overestimating the size of the tumor. Overall the intensity of BLI signals was inversely proportional to the depth of the tumor in the mouse body, and not relevant for tumor amount determination. These findings have previously been reported in a murine model of lung inflammation [10]. Tomographic luminescence imaging systems are now evaluated with the aim to recover BLI deep signals inside the mouse body, nevertheless with persistent difficulties regarding quantification [32, 33].

On the other hand, partial volume effect reduces the sensitivity of detection of PET/CT for very small lesions. The spatial resolution of our system being 1.4 mm, we could not visualize inframillimetric tumor lesions in the lungs on day 8 (only 4 lung nodules sized 0.5 mm were detected thanks to the CT). Conversely on day 17 PET detected 4 tumor sites more than BLI imaging, since the lesions reached at least 1 mm in size.

However PET/CT quantification of %ID/g could affirm lower tumor involvement in the treated group as compared to the control group on day 17, which was confirmed by *ex-vivo* counting of the tumors. Whereas the difference between the number of lesions in G1 and G2 did not reach significance because of much higher standard deviations. So in this study performed in a small number of animals, [^{18}F]MEL050-PET/CT detected significant therapeutic effect of LZDP earlier than BLI. This is of interest to reduce the number of animals used and to shorten the therapeutic protocols.

Other PET radiotracers than [^{18}F]MEL050 could be used especially [^{18}F]FDG which is used for therapy monitoring of cancers in patients [21, 23-25]. We chose [^{18}F]MEL050 because [^{18}F]MEL050 uptake in pigmented melanoma is correlated to the number of cancer cells. So [^{18}F]MEL050-PET/CT signals represent the same entity than BLI, ie cancer cells amount. Also in our previous study comparing [^{18}F]FDG PET/CT and [^{18}F]MEL050-PET/CT in the same animal model, despite %ID/g of [^{18}F]FDG in lung tumors was comparable to that of [^{18}F]MEL050 (3.20±2.43 vs 2.98±1.93, NS), those lesions were more visible with [^{18}F]MEL050 than with [^{18}F]FDG because of lower non-specific background activity (0.27±0.04 vs 1.64±0.27, P< 10-5) [18]. Moreover the use of [^{18}F]FDG imposes to verify that changes in glucose uptake by the tumors are related to slower growth. Indeed, early decrease in glucose metabolism may not always be predictive of treatment efficiency [12].

Limitation of the study

Six animals per group were planned in the study design. This number was reduced because IV injection of the radiotracer failed in 2 mice per group. However the difference between groups on PET/CT reached statistical significance and the therapeutic effect of the peptide could be affirmed before sacrifice. *Ex vivo* quantitative biodistribution of [^{18}F]MEL050 by organs and tumors counting after excision was not performed. However we estimated from previous work in our laboratory that we could rely on the quantitative data obtained from *in vivo* PET images since these latter are highly correlated to *ex vivo* counting (quasi no attenuation with positron emitters). Also the purpose of this study was *in vivo* imaging reliability to decide when to stop the experiment.

Conclusion

In this study performed in a small number of mice with metastatic pigmented melanoma, [^{18}F]MEL050-PET/CT quantification allowed to

affirm non-invasively significant anti-tumor effect of LZDP therapy whereas BLI imaging did not. BLI quantification was not accurate because of deep localization of the lesions. Also, PET/CT allowed precise localization of tumor lesions. So we conclude that PET/CT imaging is useful to reduce the number of animals and to shorten therapy evaluation experiments in our model, as well as in metastatic models grafted with cells not transfected with luciferase gene.

Acknowledgements

We thank Dr Véronique Parietti for assistance in BLI at the IUH technological platform. We thank Dr Marie Dutreix (Institute Curie) for kindly providing us the B16-F10-luc2 cells. We thank Inserm-Transfert and SATT IDF Innov for funding.

Disclosure of conflict of interest

None.

Address correspondence to: Laure Sarda-Mantel, Unité Claude Kellershohn, Institut Universitaire d'Hématologie, Bâtiment Hayem Hopital St-Louis, 1 Avenue Claude Vellefaux, Paris 75010, France. E-mail: laure.sarda@inserm.fr

References

[1] National Cancer Institute, Surveillance, Epidemiology, and End Results Program. http://seer.cancer.gov/statfacts/html/melan.html.

[2] Institut National du Cancer (INCa), rapport 1018 - Incidence projetée en 2015 du mélanome cutané, http://lesdonnees.e-cancer.fr/les-fiches-de-synthese/1-types-cancer/14-melanome-cutane/50-incidence-france-melanome-cutane.html.

[3] Mouawad R, Sebert M, Michels J, Bloch J, Spano JP, Khayat D. Treatment for metastatic malignant melanoma: old drugs and new strategies. Crit Rev Oncol Hematol 2010; 74: 27-39.

[4] Boyle GM. Therapy for metastatic melanoma: an overview and update. Expert Rev Anticancer Ther 2011; 11: 725-37.

[5] Schadendorf D, van Akkooi ACJ, Berking C, Griewank KG, Gutzmer R, Hauschild A, Stang A, Roesch A, Ugurel S. Melanoma. Lancet 2018; 392: 971-984.

[6] Faye A, Poyet JL. Targeting AAC-11 in cancer therapy. Expert Opin Ther Targets 2010; 14: 57-65.

[7] Morris EJ, Michaud WA, Ji JY, Moon NS, Rocco JW, Dyson NJ. Functional identification of Api5 as a suppressor of E2F-dependent apoptosis in vivo. PLoS Genet 2006; 2: e196.

[8] Rigou P, Piddubnyak V, Faye A, Rain JC, Michel L, Calvo F, Poyet JL. The antiapoptotic protein AAC-11 interacts with and regulates acinus-mediated DNA fragmentation. EMBO J 2009; 28: 1576-88.

[9] Jagot-Lacoussiere L, Kotula E, Villoutreix BO, Bruzzoni-Giovanelli H, Poyet JL. A cell-penetrating peptide targeting AAC-11 specifically induces cancer cells death. Cancer Res 2016; 76: 5479-90.

[10] Hadina S, Wohlford-Lenane CL, Thorne PS. Comparison of in vivo bioluminescence imaging and lavage biomarkers to assess pulmonary inflammation. Toxicology 2012; 291: 133-8.

[11] Bao X, Wang MW, Luo JM, Wang SY, Zhang YP, Zhang YJ. Optimization of early response monitoring and prediction of cancer antiangiogenesis therapy via noninvasive PET molecular imaging strategies of multifactorial bioparameters. Theranostics 2016; 6: 2084-2098.

[12] Tegnebratt T, Ruge E, Bader S, Ishii N, Aida S, Yoshimura Y, Ooi CH, Lu L, Mitsios N, Meresse V, Mulder J, Pawlak M, Venturi M, Tessier J, Stone-Elander S. Evaluation of efficacy of a new MEK inhibitor, RO4987655, in human tumor xenografts by [^{18}F]FDG-PET imaging combined with proteomic approaches. EJNMMI Res 2014; 4: 34.

[13] Schüle SC, Eigentler TK, Garbe C, la Fougère C, Nikolaou K, Pfannenberg C. Influence of ^{18}F-FDG PET/CT on therapy management in patients with stage III/IV malignant melanoma. Eur J Nucl Med Mol Imaging 2016; 43: 482-8.

[14] Chezal JM, Papon J, Labarre P, Lartigue C, Galmier MJ, Decombat C, Chavignon O, Maublant J, Teulade JC, Madelmont JC, Moins N. Evaluation of radiolabeled (hetero) aromatic analogues of N-(2-diethylaminoethyl)-4-iodobenzamide for imaging and targeted radionuclide therapy of melanoma. J Med Chem 2008; 51: 3133-44.

[15] Maisonial A, Kuhnast B, Papon J, Boisgard R, Bayle M, Vidal A, Auzeloux P, Rbah L, Bonnet-Duquennoy M, Miot-Noirault E, Galmier MJ, Borel M, Askienazy S, Dollé F, Tavitian B, Madelmont JC, Moins N, Chezal JM. Single photon emission computed tomography/positron emission tomography imaging and targeted radionuclide therapy of melanoma: new multimodal fluorinated and iodinated radiotracers. J Med Chem 2011; 54: 2745-2766.

[16] Cachin F, Miot-Noirault E, Gillet B, Isnardi V, Labeille B, Payoux P, Meyer N, Cammilleri S, Gaudy C, Razzouk-Cadet M, Lacour JP, Granel-Brocard F, Tychyj C, Benbouzid F, Grange JD, Baulieu F, Kelly A, Merlin C, Mestas D, Gachon

F, Chezal JM, Degoul F, D'Incan M. 123I-BZA2 as a melanin-targeted radiotracer for the identification of melanoma metastases: results and perspectives of a multicenter phase III clinical trial. J Nucl Med 2014; 55: 15-22.

[17] Denoyer D, Greguric I, Roselt P, Neels OC, Aide N, Taylor SR, Katsifis A, Dorow DS, Hicks RJ. High-contrast PET of melanoma using ^{18}F-MEL050, a selective probe for melanin with predominantly renal clearance. J Nucl Med 2010; 51: 441-447.

[18] Rizzo-Padoin N, Chaussard M, Vignal N, Kotula E, Tsoupko-Sitnikov V, Vaz S, Hontonnou F, Liu WQ, Poyet JL, Vidal M, Merlet P, Hosten B, Sarda-Mantel L. [^{18}F]MEL050 as a melanin-targeted PET tracer: Fully automated radiosynthesis and comparison to ^{18}F-FDG for the detection of pigmented melanoma in mice primary subcutaneous tumors and pulmonary metastases. Nucl Med Biol 2016; 43: 773-780.

[19] Greguric I, Taylor S, Pham T, Wyatt N, Jiang CD, Bourdier T, et al. Radiosynthesis of a novel PET fluoronicotinamide for melanoma tumour PET Imaging; [^{18}F]MEL050. Australian J Chem 2011; 64: 873.

[20] Rbah-Vidal L, Vidal A, Besse S, Cachin F, Bonnet M, Audin L, Askienazy S, Dollé F, Degoul F, Miot-Noirault E, Moins N, Auzeloux P, Chezal JM. Early detection and longitudinal monitoring of experimental primary and disseminated melanoma using [^{18}F]ICF01006, a highly promising melanoma PET tracer. Eur J Nucl Med Mol Imaging 2012; 39: 1449-1461.

[21] Towsend D, Cheng Z, Georg D, Drexler W, Moser E. Grand challenges in biomedical physics. Frontiers in Physics 2013; 1: 1-6.

[22] Karls S, Shah H, Jacene H. PET/CT for lymphoma post-therapy response assessment in other lymphomas, response assessment for autologous stem cell transplant, and lymphoma follow-up. Semin Nucl Med 2018; 48: 37-49.

[23] Kobe C, Dietlein M, Hellwig D. PET/CT for lymphoma post-therapy response assessment in hodgkin lymphoma and diffuse large b-cell lymphoma. Semin Nucl Med 2018; 48: 28-36.

[24] Gallamini A, Zwarthoed C. Interim FDG-PET imaging in lymphoma. Semin Nucl Med 2018; 48: 17-27.

[25] MacManus M, Everitt S, Schimek-Jasch T, Li XA, Nestle U, Kong FS. Anatomic, functional and molecular imaging in lung cancer precision radiation therapy: treatment response assessment and radiation therapy personalization. Transl Lung Cancer Res 2017; 6: 670-688.

[26] Su H, Seimbille Y, Ferl GZ, Bodenstein C, Fueger B, Kim KJ, Hsu YT, Dubinett SM, Phelps ME, Czernin J, Weber WA. Evaluation of [^{18}F] gefitinib as a molecular imaging probe for the assessment of the epidermal growth factor receptor status in malignant tumors. Eur J Nucl Med Mol Imaging 2008; 35: 1089-99.

[27] Park SS, Chunta JL, Robertson JM, Martinez AA, Oliver Wong CY, Amin M, Wilson GD, Marples B. MicroPET/CT imaging of an orthotopic model of human glioblastoma multiforme and evaluation of pulsed low-dose irradiation. Int J Radiat Oncol Biol Phys 2011; 80: 885-92.

[28] Nedergaard MK, Michaelsen SR, Urup T, Broholm H, El Ali H, Poulsen HS, Stockhausen MT, Kjaer A, Lassen U. ^{18}F-FET microPET and microMRI for anti-VEGF and anti-PlGF response assessment in an orthotopic murine model of human glioblastoma. PLoS One 2015; 10: e0115315.

[29] Oyama N, Hasegawa Y, Kiyono Y, Kobayashi M, Fujibayashi Y, Ponde DE, Dence C, Welch MJ, Yokoyama O. Early response assessment in prostate carcinoma by ^{18}F-fluorothymidine following anticancer therapy with docetaxel using preclinical tumour models. Eur J Nucl Med Mol Imaging 2011; 38: 81-9.

[30] Brepoels L, De Saint-Hubert M, Stroobants S, Verhoef G, Balzarini J, Mortelmans L, Mottaghy FM. Dose-response relationship in cyclophosphamide-treated B-cell lymphoma xenografts monitored with [^{18}F]FDG PET. Eur J Nucl Med Mol Imaging 2010; 37: 1688-95.

[31] Nguyen QD, Smith G, Glaser M, Perumal M, Arstad E, Aboagye EO. Positron emission tomography imaging of drug-induced tumor apoptosis with a caspase-3/7 specific [^{18}F]-labeled isatin sulfonamide. Proc Natl Acad Sci U S A 2009; 106: 16375-80.

[32] Cao X, Gong Y, Li Y, Zhu S, Zhang X, Zhan Y, Kang F, Wang J, Liang J. Persistent luminescence tomography for small animal imaging. Biomed Opt Express 2017; 8: 1466-1476.

[33] Gao P, Pu H, Rong J, Zhang W, Liu T, Liu W, Zhang Y, Lu H. Resolving adjacent nanophosphors of different concentrations by excitation-based cone-beam X-ray luminescence tomography. Biomed Opt Express 2017; 8: 3952-3965.